Article

DFT Insight to Ag$_2$O Modified InN as SF$_6$-N$_2$ Mixture Decomposition Components Detector

Haibo Dong, Wenjun Li, Muhammad Junaid *, Zhuo Lu, Hao Luo and Weihu Sun

School of Electrical Engineering, China University of Mining and Technology, Xuzhou 221116, China
* Correspondence: junaid@cumt.edu.cn; Tel.: +86-130-7293-7315

Abstract: In gas-insulated switchgear (GIS), partial discharge (PD) can be monitored by detecting sulfur hexafluoride-nitrogen (SF$_6$-N$_2$) decomposition components. In this paper, silver oxide (Ag$_2$O) modification was introduced to improve the gas-sensing properties of graphene-like indium nitride (InN). The adsorption process of NO$_2$, SO$_2$F$_2$, SOF$_2$ and SOF$_4$ on Ag$_2$O-InN was simulated based on the first principles calculation and density functional theory (DFT). The gas sensing mechanism was revealed by density of states theory and molecular orbital theory. It is found that Ag$_2$O doping greatly improves the adsorption properties of InN to NO$_2$ and SOF$_2$ molecules. The adsorption capacity of Ag$_2$O-InN to the four gas molecules is: NO$_2$ > SOF$_2$ > SOF$_4$ > SO$_2$F$_2$. All adsorptions can proceed spontaneously, and the gas molecules are electron donors and Ag$_2$O-InN is an electron acceptor. Through the analysis of recovery time, it is found that NO$_2$ is difficult to desorb from the substrate due to the significant adsorption energy of −2.201 eV, while SOF$_4$, SOF$_2$ and SO$_2$F$_2$ have a moderate adsorption energy of −0.185 eV, −0.754 eV and 0.173 eV and extremely short desorption time. The conductivity of the whole system changed after these four gases were adsorbed on the Ag$_2$O-InN monolayer. In summary, Ag$_2$O-InN can be used as NO$_2$ adsorbent and gas sensors to detect SOF$_4$, SOF$_2$ and SO$_2$F$_2$. This paper provides a method for on-line monitoring of partial discharge in GIS.

Keywords: Ag$_2$O-doped InN; DFT; gas-sensing; SF$_6$-N$_2$ decomposition components

1. Introduction

Ensuring the safety and stability of gas-insulated switchgear (GIS) operation is the focus of the power system [1]. In GIS, SF$_6$ has become the most popular insulating gas due to its superior insulation performance and arc extinguishing performance [2–6]. However, with the development of society, the use of SF$_6$ increasingly violates the requirements of production and environmental friendliness [7–9]. For example, SF$_6$ has high liquefaction temperature, and under a nonuniform electric field, its dielectric strength will drop sharply [10,11]. As a kind of gas that causes the greenhouse effect, it is harmful to the environment [12]. Therefore, in the future, the use of SF$_6$ shows a limited trend. How to reduce the use of SF$_6$ in the power system is an urgent problem to be solved [13,14]. SF$_6$-gas mixtures instead of pure SF$_6$ can improve technical and economic performance [15–18]. SF$_6$-N$_2$ gas mixture is a great alternative, which can reduce the use of SF$_6$ while ensuring insulation performance. It was found that the mixture containing 30% SF$_6$ can be applied to GIS bus [19]. Partial discharge (PD) can cause insulation degradation and endanger the life of GIS [20]. Under PD, the SF$_6$-N$_2$ mixture decomposes mainly as SOF$_2$, SO$_2$, SO$_2$F$_2$, SOF$_4$, CF$_4$, CO$_2$, NO, NO$_2$ and NF$_3$ [21]. PD failure can be judged by detecting characteristic gases of NO$_2$, SO$_2$F$_2$, SOF$_2$ and SOF$_4$. SOF$_2$ and SO$_2$F$_2$ are the most common, and the sensitivity of detecting the two gases by gas chromatography can reach 1 ppmv [22].

Undoped InN is an n-type wide band gap semiconductor, a graphene-like material with excellent performance, which makes up for the defect of the zero band gap of graphene and becomes a research hotspot. According to the X-ray diffractometer (XRD) analysis, Zhang et al. [23] reported the influence of substrate temperature (Ts) on the growth of InN

thin films on indium tin oxide (ITO) substrates, and clarified that gradually increasing the temperature above 200 °C is beneficial to the growth of InN (101) plane. Due to the graphene-like properties of InN, a new-type modified InN gas sensor can be developed to detect the SF_6-N_2 decomposition components. Studies showed the effect of transition metal (Cr, Fe, Ni, Mn and Co) doping on InN [24–26]. Metal oxide doping can be used to improve the gas sensing properties of materials in previous studies. G. Korotcenkov showed that the selectivity and sensitivity of SnO_2 and In_2O_3 thin films to gases can be improved by structural engineering [27]. Xu Pan et al. revealed that ZnO and CuO doped graphene has good adsorption and sensing properties for SO_2, SOF_2, and SO_2F_2 [28]. Hong Liu et al. showed that Ag_2O-doped MoSe is a potential SF_6 decomposition products sensor [29]. However, there is little study on the gas sensitivity studies of Ag_2O-modified InN monolayers to the of SF_6-N_2 decomposition components.

In this work, pristine and Ag_2O doped InN monolayers are analyzed using density functional theory (DFT), focusing on the spin unrestricted electronic structure behavior. The adsorption capacity and sensing behavior of NO_2, SOF_4, SOF_2, and SO_2F_2 gas molecule on the adsorbent surface are the key research targets. Therefore, this paper simulated the adsorption process of gas molecules on the InN monolayer surface, and systematically calculated the adsorption energy, band structure, density of states (DOS), partial density of states (PDOS), and charge transfer, and thus provided a theoretical basis for the experimental development of new-type gas sensor.

2. Materials and Methods

Based on the first principle, the adsorption and gas-sensing properties of SF_6-N_2 mixture decomposition components (NO_2, SOF_4, SOF_2, SO_2F_2) on pristine and Ag_2O-doped InN are investigated in this paper. The exchange-correlation function is described by a generalized gradient approximation (GGA) with the Perdew-Burke-Ernzerhof (PBE) functional [30,31]. By constructing a $4 \times 4 \times 1$ InN supercell, the adsorption properties and doping were investigated. The Monkhorst–Pack (MP) method was used to describe the Brillouin zone, and $7 \times 7 \times 1$ k-point was set for all simulation calculations [32,33]. The energy convergence accuracy, maximum stress, and max displacement were set as 1×10^{-5} Ha, 2×10^{-3} Ha/Å, 5×10^{-3} Å, respectively. A 15 Å vacuum slab was adopted in order to prevent interactions between the adjacent layers.

The formation energy (E_{form}) describes the stability of the doped structure, and the calculation formula is as follows:

$$E_{form} = E_{Ag_2O\text{-}InN} - E_{Ag_2O} - E_{InN} \tag{1}$$

where $E_{Ag_2O\text{-}InN}$, E_{Ag_2O}, and E_{InN} are the total energy of Ag_2O-InN, isolated Ag_2O atom and pristine InN monolayer.

The adsorption capacity of the InN monolayer towards gas molecules is described by adsorption energy (E_{ads}). The E_{ads} is defined as:

$$E_{ads} = E_{gas/suf} - E_{gas} - E_{suf} \tag{2}$$

where $E_{gas/suf}$ is the total energy of absorbed pristine or Ag_2O-doped InN system, and E_{suf}, E_{gas} represents the total energy of pristine or doped InN and isolated gas molecule, respectively.

In addition, Mulliken analysis was considered to analyze the mechanism of charge transfer (Q_t) throughout the work. Q_t of each gas adsorption process can be calculated by the following equation:

$$Q_t = Q_{gas/suf} - Q_{gas} \tag{3}$$

$Q_{gas/suf}$ and Q_{gas} denotes the charge transfer amount after adsorption carried by the gas and isolated gas, respectively. If Q_t is negative, that the substrate material loses electrons.

$$E_g = |E_{LUMO} - E_{HOMO}| \tag{4}$$

To further analyze the energy gap (E_g) of molecular orbital, the highest occupied molecular orbit energy (E_{HOMO}) and the lowest occupied molecular orbit energy (E_{LUMO}) is investigated. E_g is defined as Equation (4).

3. Results

3.1. InN Monolayer and Gas Molecules

The optimized configurations of Ag_2O-InN monolayers are shown in Figure 1a–d, and four possible dopings are considered. The formation energies of the four kinds of Ag_2O-doped substrate material are given in Table 1, the formation energy of (d) is the largest, reaching −7.038 eV. The top view and side view of the doping mode (d) are shown in Figure 1. It is evident that the lengths of three Ag-N bonds are calculated to be 2.199 Å, 2.296 Å, and 2.227 Å, respectively. Both the triangular structure of Ag_2O molecule and the large formation energy indicate the stability of the doping mode (d), and all following studies focus on the (d) configuration.
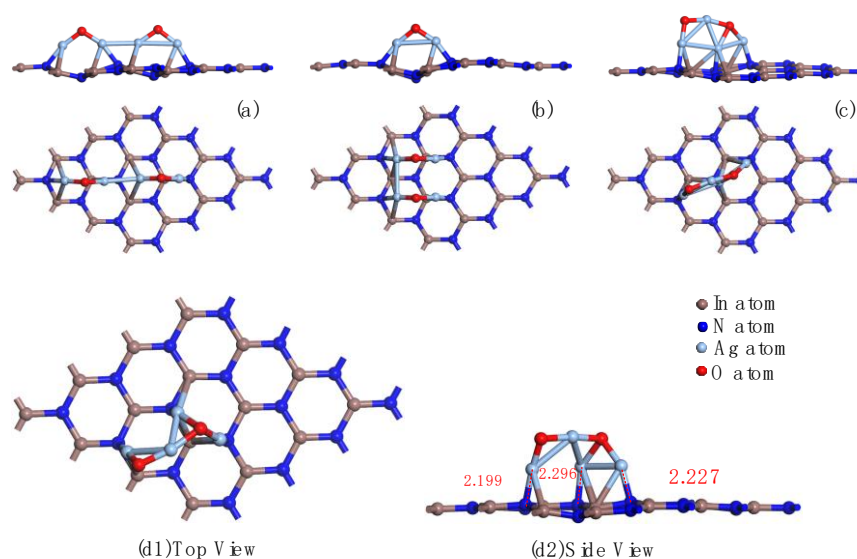
Figure 1. Four kinds of morphology of Ag_2O-InN monolayer.

Table 1. Formation energies of three Ag_2O substrate material.

Doping Site	(a)	(b)	(c)	(d)
E_{form} (eV)	−5.909	−6.459	6.663	−7.038

After structure optimization, the structure of NO_2, SOF_4, SOF_2, and SO_2F_2 molecules are demonstrated in Figure 2a–d. The N–O bond of NO_2 molecule is 1.210 Å with a planar V-shaped structure, and O-N-O bond angle is 133.489° (Figure 2a). As shown in Figure 2b, bond lengths of S=O, S-F1, and S-F2 in distorted triangular bipyramid SOF_4 are 1.444 Å, 1.655 Å and 1.610 Å while the bond angle of O=S-F1 and F1-S-F2 is 97.897° and 85.558°, respectively. Obviously, in the planar triangular SOF_2, the S-O bond length (1.461 Å) is shorter than the S-F bond length (1.670 Å), and the bond angles of O-S-F and F-S-F are 107.164° and 93.050°, as shown in Figure 2c. Besides, SO_2F_2 molecule exhibits a regular tetrahedron, with O-S bond length of 1.443 Å and O-F bond length of 1.612 Å. The angles of O-S-O bond, O-S-F and F-S-F in SO_2F_2 are 102.703°, 107.775° and 90.409°, respectively. It is worth noting that in SOF_4, SOF_2, and SO_2F_2, the length of the S-F bond is negatively correlated with the electronegativity of F atom.
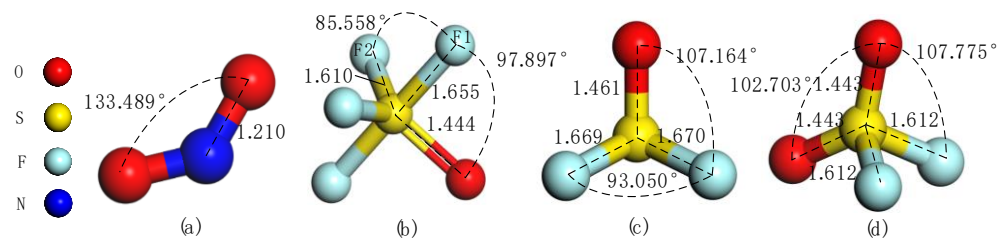
Figure 2. Structures of (**a**) NO$_2$, (**b**) SOF$_4$, (**c**) SOF$_2$ and (**d**) SO$_2$F$_2$ molecules.

3.2. SF$_6$-N$_2$ Decomposition Components Adsorption on InN Monolayer

Figure 3 and Table 2 exhibit the most stable adsorption configurations of SF$_6$-N$_2$ decomposition components on undoped InN. It can be seen that adsorption distances of NO$_2$, SOF$_4$, SOF$_2$, and SO$_2$F$_2$ on the InN monolayer are 3.132 Å, 2.986 Å, 3.077 Å and 3.297 Å, respectively. SOF$_4$ tends to be adsorbed on the InN monolayer by F atom (seen in Figure 3b), and the absolute value of the adsorption energy (2.242 eV) is much greater than 0.8 eV, indicating that it is strong chemisorption. Apart from that, the adsorption energy is −0.839 eV in NO$_2$ system, −0.483 eV in SOF$_2$ system, and −0.380 eV in SO$_2$F$_2$ system. Tiny adsorption energy means weak adsorption. Additionally, for the NO$_2$, SOF$_4$, SOF$_2$ and SO$_2$F$_2$ adsorption, the charge transfer direction is from the InN monolayer to the gas molecule, as further verified by the −0.400 *e*, −1.188 *e*, −0.022 *e* and −0.007 *e* of these systems. The negative charge transfers of O atoms and F atoms indicate that they are electron acceptors. For SOF$_2$ and SO$_2$F$_2$ adsorption, the tiny charge transfer mainly occurs in the gas molecules themselves, further confirming the weak interaction, which is consistent with the adsorption energy analysis.
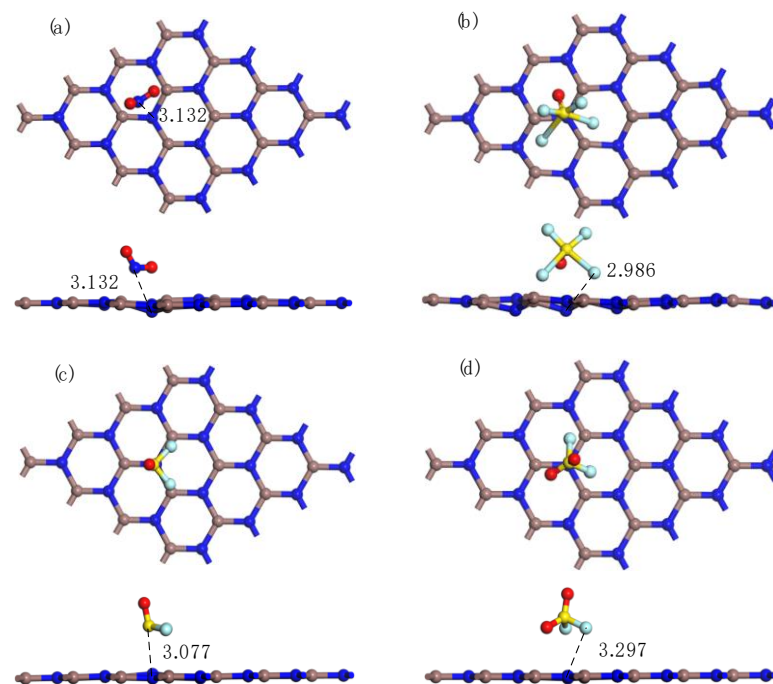
Figure 3. Adsorption structure of (**a**) NO$_2$, (**b**) SOF$_4$, (**c**) SOF$_2$ and (**d**) SO$_2$F$_2$ molecules adsorbed on InN monolayer.

Table 2. Adsorption parameters of NO_2, SOF_4, SOF_2 and SO_2F_2 on undoped InN monolayer.

Adsorption Structures	Figure	Adsorption Distance	E_{ads}	Atom	Mulliken Charge	Q_t
NO_2/InN	Figure 3a	3.132 Å	−0.839 eV	N	0.217 *e*	−0.400 *e*
				O	−0.369 *e*	
				O	−0.248 *e*	
SOF_4/InN	Figure 3b	2.986 Å	−2.242 eV	S	0.794 *e*	−1.188 *e*
				O	−0.329 *e*	
				F	−0.275 *e*	
				F	−0.549 *e*	
				F	−0.293 *e*	
				F	−0.536 *e*	
SOF_2/InN	Figure 3c	3.077 Å	−0.483 eV	S	0.750 *e*	−0.022 *e*
				O	−0.231 *e*	
				F	−0.269 *e*	
				F	−0.272 *e*	
SO_2F_2/InN	Figure 3d	3.297 Å	−0.380 eV	S	0.896 *e*	−0.007 *e*
				O	−0.218 *e*	
				O	−0.244 *e*	
				F	−0.222 *e*	
				F	−0.219 *e*	

In brief, the negative adsorption energy indicates that the InN monolayer adsorbs NO_2, SOF_4, SOF_2, and SO_2F_2 molecule spontaneously. InN monolayer substrate is electron donor, and gas molecules are electron acceptors. The adsorption capacity of InN monolayer to SF_6-N_2 decomposition components is in the following order: $SOF_4 > NO_2 > SOF_2 > SO_2F_2$.

3.3. SF_6-N_2 Decomposition Components Adsorption on Ag_2O-InN Monolayer

To analyze the adsorption behaviors of Ag_2O-InN to NO_2, SOF_4, SOF_2, SO_2F_2 molecules, the gas molecules are approached to the Ag_2O-InN monolayer, and the most stable adsorption structure and adsorption parameters are shown in Figure 4 and Table 3.

It can be seen from Figure 4 that the four gas molecules all undergo slight deformation on Ag_2O-InN monolayer. The adsorption energies of NO_2, SOF_4, SOF_2, and SO_2F_2 molecules on Ag_2O-InN are −2.021 eV, −0.185 eV, −0.754 eV and −0.173 eV, respectively. Obviously, after Ag_2O doping, the adsorption energy of NO_2 and SOF_2 increase, on the contrary, the adsorption energies of SOF_4 and SO_2F_2 decrease. Meanwhile, the charge transfer of NO_2, SOF_4, SOF_2, and SO_2F_2 molecules on Ag_2O-InN are −0.174 *e*, −0.028 *e*, −0.279 *e* and −0.015 *e*, respectively. The negative charge transfer indicates that the gas molecules are the electron acceptors and Ag_2O-InN is the electron donor. Among the four gases, only SOF_2 and SO_2F_2 adsorption resulted in an increase in the charge transfer quantity compared undoped InN. In NO_2 adsorption, the NO_2 molecule is activated and absorbed by O atom, forming a N-O bond (1.383 Å) with Ag_2O-InN. None of the other three gases formed bonds with Ag_2O-InN. From the large adsorption energy, small adsorption distance, and large charge transfer, it can be inferred that the NO_2 adsorption is chemisorption. As for SOF_2 adsorption, the adsorption distance is 2.143 Å, which is smaller than that on pristine InN. It is worth noting that the absolute value of adsorption energy of SOF_2 is larger than 0.7 eV, which also belongs to chemisorption. For SOF_4 and SO_2F_2 adsorption, it is inferred that they belong to physisorption by the tiny adsorption energy, large adsorption distance and small charge transfer. In conclusion, NO_2, SOF_4, SOF_2, SO_2F_2 molecules tend to adsorb on Ag_2O molecules in the Ag_2O-InN monolayer. The adsorption capacity of the four gas molecules is: $NO_2 > SOF_2 > SOF_4 > SO_2F_2$.
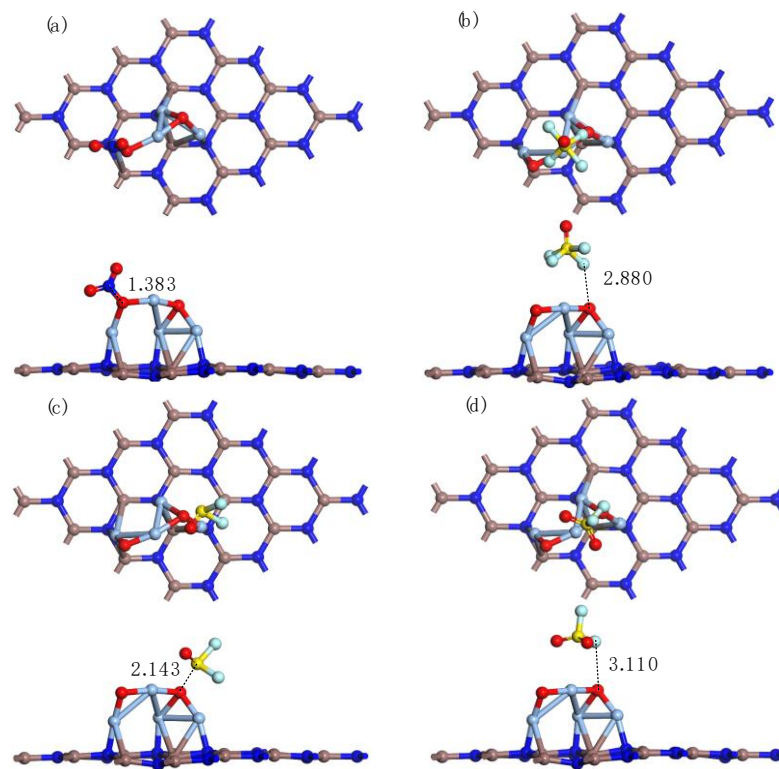
Figure 4. Adsorption structure of (**a**) NO_2, (**b**) SOF_4, (**c**) SOF_2 and (**d**) SO_2F_2 molecules adsorbed on Ag_2O-InN monolayer.

Table 3. Adsorption parameters of NO_2, SOF_4, SOF_2 and SO_2F_2 on Ag_2O-InN monolayer.

Gas Molecules	Figure	Adsorption Distance (Å)	E_{ads} (eV)	Charge Transfer (Q_t)
NO_2	Figure 4a	1.383	−2.021	−0.174 e
SOF_4	Figure 4b	2.880	−0.185	−0.028 e
SOF_2	Figure 4c	2.143	−0.754	−0.279 e
SO_2F_2	Figure 4d	3.110	−0.173	−0.015 e

3.4. Analysis of Density of States of Gas Adsorption on Ag$_2$O-InN

Figure 5 presents the DOS (density of states) and PDOS (partial density of states) before and after NO_2, SOF_4, SOF_2, SO_2F_2 are absorbed on Ag_2O-InN monolayer. The outermost electrons of atoms have the greatest influence on the adsorption process, so their PDOS was analyzed and compared. For NO_2 adsorption, the redistribution of TDOS is dramatic. The clear hybridization of N-*2p* and O-*2p* at −12 eV, −9 eV, 2 eV is consistent with the phenomenon of bonding between N atom and O atom. Similarly, SOF_2 undergoes redistribution of TDOS and strong orbital hybridization. The strong orbital hybridization indicates that the adsorption reaction of NO_2 and SOF_2 is strong, which is consistent with the conclusion that they are chemisorption. As for the SOF_4 and SO_2F_2 adsorption, a slight redistribution of TDOS occurred, and PDOS did not reflect the bonding information, which is consistent with Figure 4. The new peaks between −5~−12.5 eV mainly caused by F-*2p*, S-*2p* and O_{gas}-*2p*, while the contribution of Ag-*4d* is mainly located at the Fermi level. However, the adsorption of these two molecules on the substrate was strong physisorption. In short, after gas adsorption, the redistribution of TDOS proves the existence of charge transfer. The adsorption behavior will change the conductivity of adsorption system, which provide the feasibility of preparing Ag_2O modified InN gas sensor.
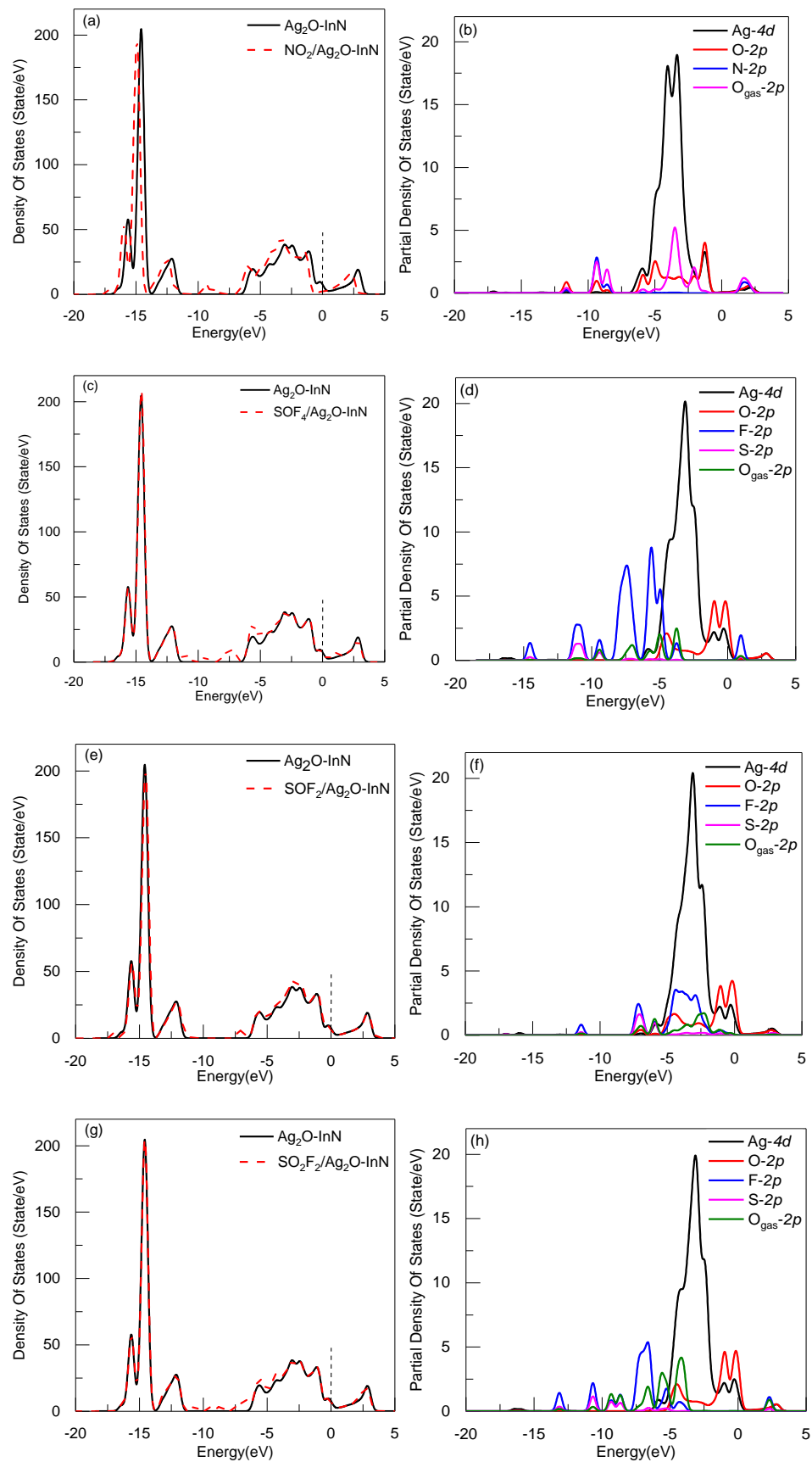
Figure 5. DOS (**a,c,e,g**) and PDOS (**b,d,f,h**) of before and after gas molecules adsorption on Ag$_2$O-InN. The dotted line represents the Fermi energy.

3.5. Molecular Orbital Analysis and Recovery Time of Gas Adsorption on Ag₂O-InN

According to the molecular orbital theory, the HOMO and LUMO of Ag$_2$O-InN and the four gas adsorption systems were analyzed, as shown in Figure 6. The distribution of HOMO and LUMO reflects the electronic behavior during the adsorption process. The energy gap between HOMO and LUMO reveals the ability of electron transition from the valence band to conduction band, and is an important parameter to measure the conductivity of adsorption system. Before gas adsorption, HOMO and LUMO are mainly located on Ag$_2$O dopant, Ag$_2$O is the active site on the InN monolayer. After adsorption, the LUMO of NO$_2$ adsorption system is mainly distributed on Ag$_2$O dopant, and the HOMO of SOF$_4$, SOF$_2$ and SO$_2$F$_2$ adsorption systems is mainly located on Ag$_2$O dopant. In addition, the gas adsorption leads to a small reduction in energy gaps compared to the unadsorbed Ag$_2$O-InN energy gap (1.768 eV). Energy gaps of the NO$_2$, SOF$_4$, SOF$_2$ and SO$_2$F$_2$ system drop to 1.669 eV, 0.952 eV, 1.659 eV and 1.742 eV, respectively. All gas adsorptions lead to enhancement in system conductivity. Especially, the energy gap of SOF$_4$ system is 0.816 eV narrower than that of non-adsorbed Ag$_2$O-InN, indicating a much better conductivity. The conductivity of the four adsorption systems is arranged as: SOF$_4$ > SOF$_2$ > NO$_2$ > SO$_2$F$_2$. The change of conductivity after gas adsorption provides a theoretical basis for the preparation of resistive gas sensors.
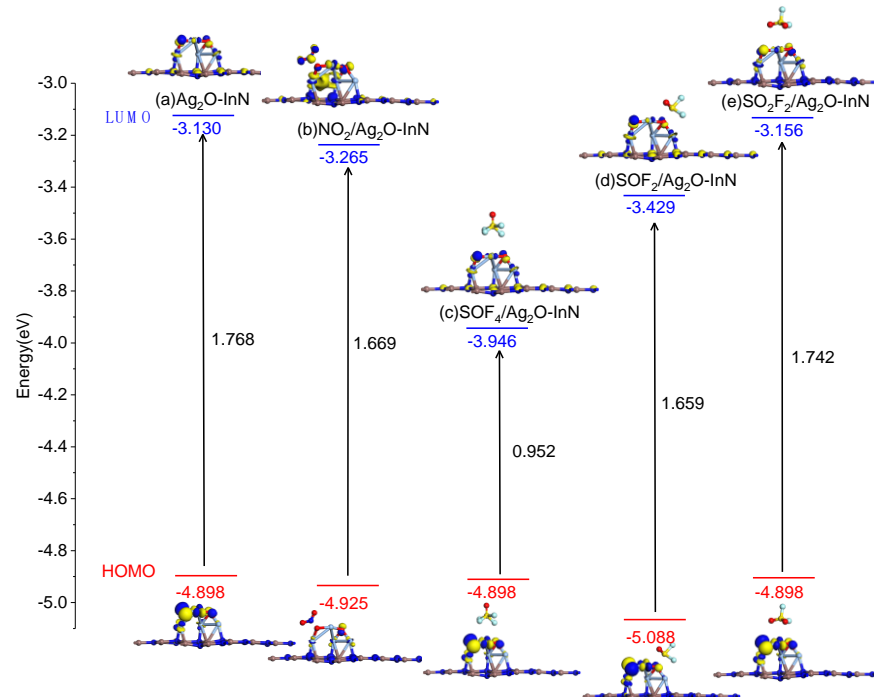
Figure 6. HOMO and LUMO of Ag$_2$O-InN and adsorption system.

In order to explore the desorption capacity of Ag$_2$O-InN, the recovery time of gas molecules was calculated by Equation (5).

$$\tau = \gamma^{-1} \exp\left(-E_{ads}/K_B T\right) \tag{5}$$

γ, K_B and T represent the attempt frequency ($10^{-12} s^{-1}$), Fahrenheit temperature (298 K, 348 K and 418 K) and Boltzmann constant (8.62×10^{-5} eV K^{-1}), respectively. The recovery times of the four gas molecules at 298 K, 348 K and 418 K are shown in Table 4. Due to the large adsorption energy and strong chemisorption, the recovery time of NO$_2$ at 298K is 1.474×10^{23} s, indicating that NO$_2$ cannot desorb form Ag$_2$O-InN. Therefore, Ag$_2$O-InN is suitable as a NO$_2$ scavenger, but not as a NO$_2$ sensor. However, the recovery time of SOF$_4$, SOF$_2$ and SO$_2$F$_2$ on Ag$_2$O-InN is extremely short, and Ag$_2$O-InN has good reusability as a sensor for detecting these three gases.

Table 4. Recovery time of NO_2, SOF_4, SOF_2 and SO_2F_2 on Ag_2O-InN monolayer.

Adsorption System	K_B (K)	τ (s)
NO_2/Ag_2O-InN	298	1.474×10^{23}
	348	1.817×10^{18}
	418	2.288×10^{13}
SOF_4/Ag_2O-InN	298	1.342×10^{-8}
	348	4.768×10^{-9}
	418	1.698×10^{-9}
SOF_2/Ag_2O-InN	298	55.94
	348	8.244×10^{-1}
	418	1.225×10^{-2}
SO_2F_2/Ag_2O-InN	298	8.411×10^{-9}
	348	3.196×10^{-9}
	418	1.217×10^{-9}

4. Discussion

Based on the first principles calculation, the adsorption process of SF_6-N_2 decomposition components (NO_2, SOF_4, SOF_2, SO_2F_2) on pristine and Ag_2O-doped InN was simulated. By analyzing the adsorption energy, charge transfer, density of states, molecular orbital theory and recovery time, the adsorption mechanism of gas molecules on Ag_2O-doped InN was further revealed. Pristine InN shows strong adsorption to SOF_4 molecules, but exhibits weak adsorption to NO_2, SOF_2, and SO_2F_2 molecules. In particular, the charge transfer quantity for SOF_2 and SO_2F_2 adsorption on pristine InN are only 0.022 *e* and 0.007 *e*. The gas sensing capacity of InN to SOF_2 and SO_2F_2 is poor. Compared with undoped InN, Ag_2O-InN has a significantly higher adsorption energy for NO_2, and a significantly larger adsorption energy and charge transfer quantity for SOF_2. The large adsorption energy makes it difficult for NO_2 to desorb form Ag_2O-InN, so Ag_2O-InN is difficult to be a NO_2 sensor. At the same time, the moderate adsorption energy, large charge transfer, and obvious changes in conductivity make Ag_2O-InN a good sensor for SOF_4, SOF_2, and SO_2F_2. In conclusion, this paper not only explores the gas sensing mechanism of Ag_2O-doped InN to SF_6-N_2 decomposed components, but also provides a theoretical basis for fabricating Ag_2O-InN sensors for online monitoring of partial discharge in GIS.

5. Conclusions

This paper reveals the gas-sensing mechanism of pristine and Ag_2O-doped InN to SF_6-N_2 decomposition components. Studies show that pristine InN exhibits poor sensing ability for SF_6-N_2 decomposition components. The Ag_2O dopant is the active site on the substrate material surface, and the four gas molecules tend to be adsorbed on Ag_2O. The order of adsorption capacity is: NO_2 > SOF_2 > SOF_4 > SO_2F_2. The doping of Ag_2O dramatically increases the absolute value of the adsorption energy of NO_2 to 2.021 eV, resulting in that NO_2 cannot be desorbed from Ag_2O-InN. In addition, moderate adsorption energy, large charge transfer, and obvious conductivity change make Ag_2O-InN a potential material for the fabrication of SOF_4, SOF_2, and SO_2F_2 sensors, and the extremely short desorption time reveals the reusability of Ag_2O-InN as a gas sensor.

Author Contributions: Conceptualization and methodology, H.D.; data curation, writing—original draft, writing—review and editing, W.L.; Supervision, software, funding acquisition and resources, M.J.; formal analysis, visualization, and investigation, Z.L., H.L. and W.S. All authors have read and agreed to the published version of the manuscript.

Institutional Review Board Statement: Not applicable.

Informed Consent Statement: Not applicable.

Data Availability Statement: Not applicable.

Conflicts of Interest: The authors declare no conflict of interest.

References

1. Zhang, Q.; Gui, Y.; Qiao, H.; Chen, X.; Cao, L. Theoretical study of SF6 decomposition products adsorption on metal oxide cluster-modified single-layer graphene. *J. Ind. Eng. Chem.* **2022**, *105*, 278–290. [CrossRef]
2. Zhang, X.; Cui, H.; Gui, Y.; Tang, J. Mechanism and Application of Carbon Nanotube Sensors in SF6 Decomposed Production Detection: A Review. *Nanoscale Res. Lett.* **2017**, *12*, 177. [CrossRef]
3. Tang, B.; Tang, J.; Liu, Y.; Zeng, F. Comprehensive Evaluation and Application of GIS Insulation Condition Part 1: Selection and Optimization of Insulation Condition Comprehensive Evaluation Index Based on Multi-Source Information Fusion. *IEEE Access* **2019**, *7*, 88254–88263. [CrossRef]
4. Chen, D.; Tang, J.; Zhang, X.; Li, Y.; Liu, H. Detecting Decompositions of Sulfur Hexafluoride Using MoS2 Monolayer as Gas Sensor. *IEEE Sens. J.* **2019**, *19*, 39–46. [CrossRef]
5. Zeng, F.; Tang, J.; Xie, Y.; Zhou, Q.; Zhang, C. Experience Study of Trace Water and Oxygen Impact on SF6 Decomposition Characteristics Under Partial Discharge. *J. Electr. Eng. Technol.* **2015**, *10*, 1786–1795. [CrossRef]
6. Zeng, F.; Li, H.; Cheng, H.; Tang, J.; Liu, Y. SF6 decomposition and insulation condition monitoring of GIE: A review. *High Volt.* **2021**, *6*, 955–966. [CrossRef]
7. Wei, G.; Bai, Y.; Hu, M.; Cao, Z.; Fu, W. Research on Environmental Protection Treatment for Ex-Service SF$_6$ Adsorbent. *IEEE Access* **2020**, *8*, 93840–93849. [CrossRef]
8. Xiao, S.; Zhang, X.; Tang, J.; Liu, S. A review on SF6 substitute gases and research status of CF3I gases. *Energy Rep.* **2018**, *4*, 486–496. [CrossRef]
9. Ullah, R.; Rashid, A.; Rashid, A.; Khan, F.; Ali, A. Dielectric characteristic of dichlorodifluoromethane (R12) gas and mixture with N-2/air as an alternative to SF6 gas. *High Volt.* **2017**, *2*, 205–210. [CrossRef]
10. Onal, E. Breakdown Mechanism of Different Sulphur Hexafluoride Gas Mixtures. *Adv. Mater. Sci. Eng.* **2018**, *2018*, 3206132. [CrossRef]
11. Chen, G.; Tu, Y.; Wang, C.; Wang, J.; Yuan, Z.; Ma, G.; Wang, J.; Qi, B.; Li, C. Environment-friendly Insulating Gases for HVDC Gas-insulated Transmission Lines. *CSEE J. Power Energy Syst.* **2021**, *7*, 510–529. [CrossRef]
12. Kharal, H.S.; Kamran, M.; Ullah, R.; Saleem, M.Z.; Alvi, M.J. Environment-Friendly and Efficient Gaseous Insulator as a Potential Alternative to SF6. *Processes* **2019**, *7*, 740. [CrossRef]
13. Owens, J.; Xiao, A.; Bonk, J.; DeLorme, M.; Zhang, A. Recent Development of Two Alternative Gases to SF6 for High Voltage Electrical Power Applications. *Energies* **2021**, *14*, 5051. [CrossRef]
14. Wang, Y.; Huang, D.; Liu, J.; Zhang, Y.; Zeng, L. Alternative Environmentally Friendly Insulating Gases for SF6. *Processes* **2019**, *7*, 216. [CrossRef]
15. Li, X.; Zhao, H.; Murphy, A.B. Murphy, SF6-alternative gases for application in gas-insulated switchgear. *J. Phys. D Appl. Phys.* **2018**, *51*, 153001. [CrossRef]
16. Zhao, H.; Deng, Y.; Tian, Z. Dielectric breakdown properties of CF3I-N2 mixtures containing a small amount of SF6. *AIP Adv.* **2019**, *9*, 055031. [CrossRef]
17. Panchenko, A.N.; Tarasenko, V.F.; Beloplotov, D.V.; Panchenko, N.A.; Lomaev, M.I. Diffuse discharges in SF6 and mixtures of SF6 with H-2, formed by nanosecond voltage pulses in non-uniform electric field. *High Volt.* **2018**, *3*, 316–322. [CrossRef]
18. Dincer, M.S.; Tezcan, S.S.; Duzkaya, H. Suppression of Electron Avalanches in Ultra-Dilute SF6-N-2 Mixtures Subjected to Time-Invariant Crossed Fields. *Energies* **2018**, *11*, 3247. [CrossRef]
19. Zhou, A.; Gao, L.; Ji, X. Research and Application of SF6/N2 Mixed Gas Used in GIS Bus. *Power Syst. Technol.* **2018**, *42*, 3429–3435. [CrossRef]
20. Metwally, I. Status review on partial discharge measurement techniques in gas-insulated switchgear/lines. *Electr. Power Syst. Res.* **2004**, *69*, 25–36. [CrossRef]
21. Casanovas, A.M.; Casanovas, J. Decomposition of high-pressure (400 kPa) SF6-CO2, SF6-CO, SF6-N-2-CO2 and SF6-N-2-CO mixtures under negative dc coronas. *J. Phys. D Appl. Phys.* **2005**, *38*, 1556–1564. [CrossRef]
22. Pearson, J.; Farish, O.; Hampton, B.; Judd, M.; Templeton, D.; Pryor, B.; Welch, I. Partial discharge diagnostics for gas insulated substations. *IEEE Trans. Dielectr. Electr. Insul.* **1995**, *2*, 893–905. [CrossRef]

23. Zhang, Z.; Xiang, G.; Zhang, J.; Zhang, J.; Liu, Y.; Peng, W.; Zhou, Y.; Li, R.; Mei, M.; Zhao, Y.; et al. Preparation of InN films at different substrate temperatures and the effect of operating temperatures on the carrier transmission characteristics of p-NiO/n-InN heterojunction. *Vacuum* **2021**, *194*, 110583. [CrossRef]

24. Lin, X.; Mao, Z.; Dong, S.; Jian, X.; Han, R.; Wu, P. First-principles study on the electronic structures and magnetic properties of InN monolayer doped with Cr, Fe, and Ni. *Phys. E Low-Dimens. Syst. Nanostruct.* **2021**, *127*, 114524. [CrossRef]

25. Xu, D.; Zhao, Z.; Zhang, Y.; Lou, Y.; Li, P. Influence of valence states and vacancy defects on the magnetic properties of Mn doped InN. *Solid State Commun.* **2019**, *297*, 11–16. [CrossRef]

26. Caliskan, S.; Hazar, F. First principles study on the spin unrestricted electronic structure properties of transition metal doped InN nanoribbons. *Superlattices Microstruct.* **2015**, *84*, 170–180. [CrossRef]

27. Korotcenkov, G. Gas response control through structural and chemical modification of metal oxide films: State of the art and approaches. *Sens. Actuators B Chem.* **2005**, *107*, 209–232. [CrossRef]

28. Xu, P.; Gui, Y.; Chen, X. A DFT study of adsorption properties of SO2, SOF2, and SO2F2 on ZnO/CuO doped graphene. *Diam. Relat. Mater.* **2022**, *126*, 109103. [CrossRef]

29. Liu, H.; Xu, L.; Gui, Y.; Ran, L.; Chen, X. Adsorption properties of Ag2O–MoSe2 towards SF6 decomposed products. *Vacuum* **2021**, *189*, 110248. [CrossRef]

30. Liu, Y.; Zhou, Q.; Wang, J.; Zeng, W. Cr doped MN (M = In, Ga) monolayer: A promising candidate to detect and scavenge SF6 decomposition components. *Sens. Actuators A Phys.* **2021**, *330*, 112854. [CrossRef]

31. Delley, B. From molecules to solids with the DMol 3 approach. *J. Chem. Phys.* **2000**, *113*, 7756–7764. [CrossRef]

32. Monkhorst, H.J.; Pack, J.D. Special points for Brillouin-zone integrations. *Phys. Rev. B* **1976**, *13*, 5188–5192. [CrossRef]

33. Zhu, S.; Ma, S. Adsorption and Sensing Behaviors of Pd-Doped InN Monolayer upon CO and NO Molecules: A First-Principles Study. *Appl. Sci.* **2019**, *9*, 3390. [CrossRef]